# Lawrence Berkeley National Laboratory

## LBL Publications


### Title

Performance of plane wavefront Fizeau interferometers in power spectral density measurements with tilted plane optics


### Permalink

https://escholarship.org/uc/item/43v670kh



### Authors

Yashchuk, VV

Munechika, K

Rochester, S

et al.



### Publication Date

2024

### DOI

10.1117/12.3028336



### Copyright Information

This work is made available under the terms of a Creative Commons Attribution-NonCommercial License, available at https://creativecommons.org/licenses/by-nc/4.0/

Peer reviewed

eScholarship.org Powered by the California Digital Library University of California

# Performance of Plane Wavefront Fizeau Interferometers in Power Spectral Density Measurements with Tilted Plane Optics

V. V. Yashchuk,[a] K. Munechika,[b] S. Rochester,[c] P. Z. Takacs,[d] I. Lacey,[a] and K. Yamada[b]
[a]Advanced Light Source, LBNL, 1 Cyclotron Road, Berkeley, CA 94720, USA; [b]HighRI Optics, Inc., 5401 Broadway Terr, St. 304, Oakland, CA 94618, USA; [c]Rochester Scientific, LLC, 2041 Tapscott Avenue, El Cerrito, CA 94530, USA; [d]Surface Metrology Solutions, LLC, 19 S 1st St, Unit B901, Minneapolis, MN 55401 USA,

## ABSTRACT

Binary pseudo-random array (BPRA) test samples are useful devices for calibrating the instrument transfer function (ITF) of Fizeau interferometers, interferometric microscopes, and other optical and non-optical surface and wavefront metrology instruments. The intrinsic white noise character of the power spectral density (PSD) function of the BPRA pattern simplifies the extraction of the ITF from the measured PSD. The ITF determined in a dedicated calibration experiment can be used to reconstruct the surface height profile from the measured data, effectively enhancing the instrument's spatial resolution. For a high confidence reconstruction procedure, a reliable analytical model of the IFT is desirable. Usually, the model accounts for the contributions to the ITF related the imperfections of the instrument's optical and detector systems. Here, we experimentally demonstrate that in the case of surface height metrology with Fizeau interferometers, the PSD measurements and, therefore, the efficacy of the ITF calibration of the tool, are strongly affected by the instrument data acquisition and processing procedures, as well as by the shape of the optic under test and its alignment with respect to the interferometer.

**Keywords:** Fizeau interferometry, calibration, systematic error, retrace error, instrument transfer function, binary pseudo-random, surface metrology, x-ray optics

## 1. INTRODUCTION

For decades, plane wavefront Fizeau interferometry (PWFI) has been one of the major metrology techniques for surface characterization of x-ray optics in the low and middle spatial frequency range (see, for example, Refs. [1-3] and references therein). However, the application of the technique for metrology with large-radius tangentially-curved optics is known to be associated with a number of systematic errors. The error that arises because of the difference between the optical paths of the reference light and the light reflected off the optic under test (OUT) is the well-known retrace error [3-5]. A less-investigated source of error is geometrical distortion (GD) (see the discussion in Refs. [6,7]). Other errors in PWFI arise from limited spatial resolution, leading to systematic effects in the spatial frequency domain that are usually characterized by the instrument transfer function (ITF) [8-10]. Measurement errors of the same nature appear also in the measurements of a misaligned plane OUT.

We have developed methods for experimental calibration of a Fizeau interferometer in both the spatial and spatial-frequency domains using plane substrate test samples patterned with uniformly redundant array (URA) and highly randomized (HR) binary pseudo-random array (BPRA) designs (see Refs. [11-13] and references therein). To use these methods in our project to develop precision stitching plane wavefront Fizeau interferometry (SPWFI) metrology with long tangentially curved x-ray mirrors, we have tilted the test samples, similarly to Ref. [5], to mimic the appearance of a tangentially curved OUT. In this paper, we present the results of experimental tests and discuss the possible origins of the observed irregularities and systematic errors based on a simplified optical model and the data acquisition and processing of the of the tool. Using such techniques, we aim to reduce systematic errors to the single digit nanometer level in stitching Fizeau interferometer measurements of state-of-the-art aspherical x-ray mirrors.

*VVYashchuk@lbl.gov; phone 1 510 495-2592; www.lbl.gov

## 2. EXPERIMENTAL INVESTIGATION OF INTERFEROMETER INSTRUMENTAL TRANSFER FUNCTIONS WITH SAMPLE AT DIFFERENT TILT ANGLES

In the course of our systematic error investigations with tilted plane artifacts, we observed a dramatic change (flattening) of the 1D PSD with increasing tilt of the sample. We also observed a significant difference in the tilt dependence of the PSD in the horizontal (PSDX) and vertical (PSDY) directions. These observations have triggered a more systematic investigation of PSD measurements and ITF calibration of the two Fizeau interferometers, Zygo Verifire$^{TM}$ and Zygo DynaFiz$^{TM}$, both available at the ALS XROL [14]. The results of these investigations are summarized in the present paper.

### 2.1 DynaFiz interferometer tests for different tilt angles

Figure 1a depicts the experimental arrangement for the DynaFiz measurements with the 25-µm HR BPRA test sample [13] at different tilts in the horizontal (around the vertical axis) and the vertical (around the horizontal axis) directions. For the measurements, the interferometer was equipped with a flat transmission reference.

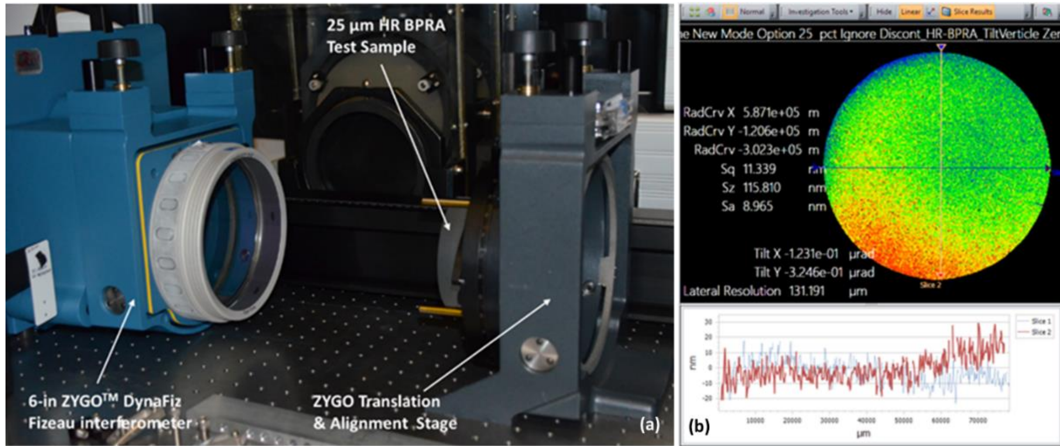


Figure 1. (a) Experimental setup of the ALS XROL Zygo DynaFiz$^{TM}$ Fizeau interferometer, equipped with a flat transmission reference, used for measurements with the 25-µm HR BPRA test sample at different tilts. (b) The surface height topography as measured with of the untilted (Tilt X ≈ –0.1 µrad, Tilt Y ≈ –0.3 µrad) test sample.

Figure 2 shows the 1D PSD in the X and Y directions measured with the 25-µm HR BPRA at different horizontal tilts [plots (a-c) with tilts of –330 µrad, no tilt, and +307 µrad, respectively] and vertical tilts [plots (d-f) with tilts of –376 µrad, no tilt, and +395 µrad, respectively]. Unlike similar measurements with the Verifire (see Sec. 2.3, below), the PSDs in Fig. 2 are not monotonic, having bumps near a spatial frequency of about 2.5 mm$^{-1}$.

At first glance, the bumps could appear to be a defocus effect (see, for example, discussion in Ref. [15]). However, this is in contradiction with the significant dependence of the bump frequency and shape on a relatively small change of the tilt angle. Indeed, the largest applied tilt of about 0.4 mrad [Fig. 2(f)] changes the sample edge-to-interferometer distance (at 50 mm from the sample center) by only ±20 µm.

In addition to the different shape, the data in Fig. 2 also show a different tilt dependence than that observed with the Verifire interferometer. With X-tilt in both the positive and negative directions, the PSDX decreases (rather than increases) and better matches (rather than diverges from) the PSDY [Fig. 2(a-c)]. On the other hand, when tilting the sample in the Y-direction [Fig. 2(d-f)], the PSDY depends on the sign of the tilt.

The origin of the anomalous PSD bumps and tilt dependences in the DynaFiz measurements is not clear, and may be the result of the data acquisition and processing algorithms built into the instrument. The "Dyna" in DynaFiz refers to the optimization of the interferometer design for dynamic measurements in the presence of vibrations or air turbulence. Unfortunately, due to its proprietary nature, information about how this is accomplished is very limited and vague. At the AMETEK/Zygo Corporation website [16], one can find primarily general statements about applications, rather than the design of the instrument. Thus, we can currently only speculate on the source of these effects in the proprietary design of the instrument.

It is possible that it is difficult to observe these effects with the use of a simple surface-step test sample [17,18] for calibration that does not provide quantitative information about the ITF over its entire spatial frequency range.

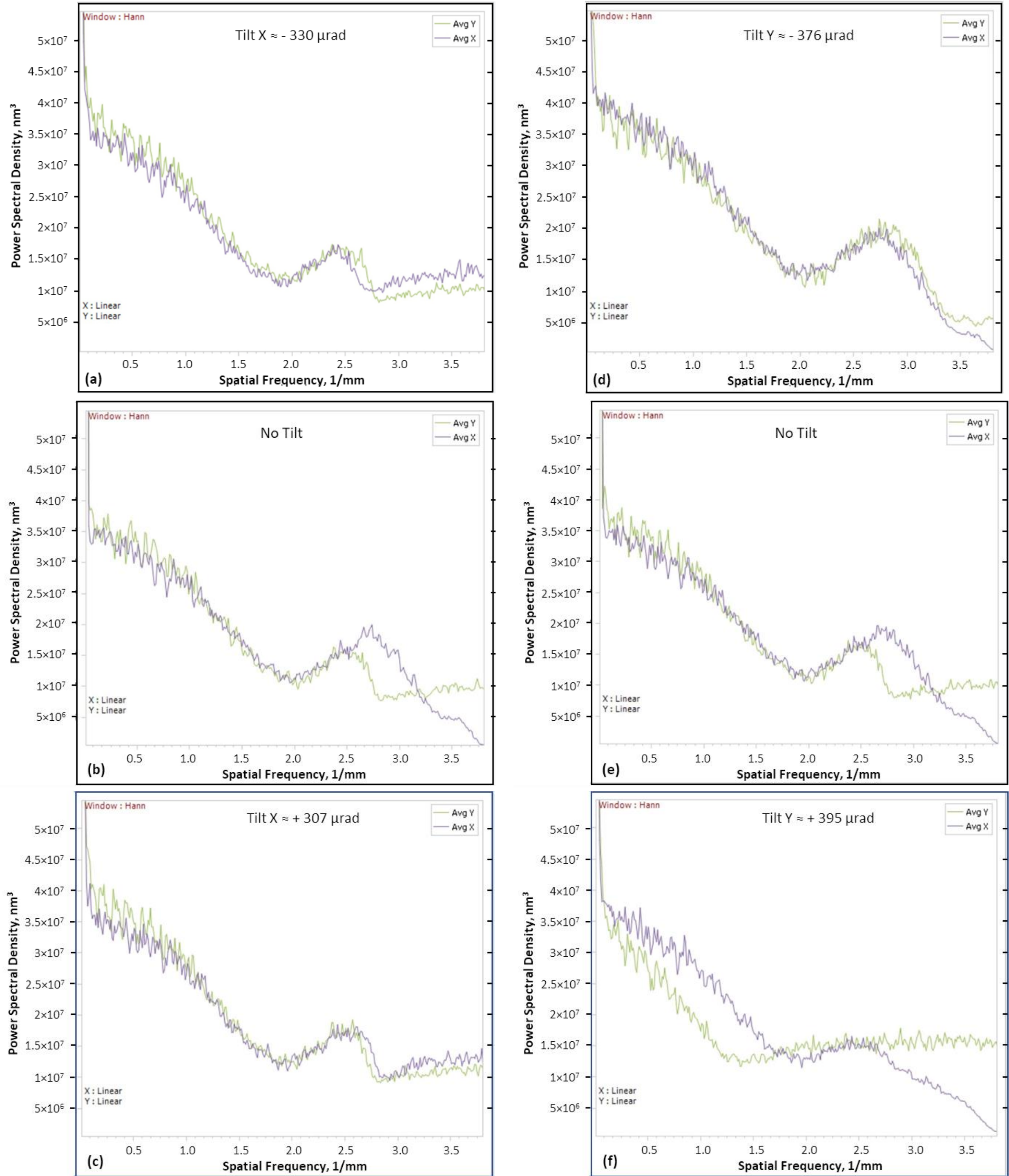


Figure 2. Zygo Mx screenshots showing PSD in the X (violet lines) and Y (green lines) directions from DynaFiz measurements with -order polynomial detrending. The BPRA test sample was at different horizontal tilts of (a) –330 µrad, (b) no tilt, and (c) +307 µrad, and vertical tilts of (d) –376 µrad, (e) no tilt, and (f) +395 µrad.

Because understanding these observations is necessary for reliable ITF calibration of the DynaFiz interferometer, we plan additional experimental tests and numerical simulations.

### 2.2 Possible origin of the PSD dependence on tilt in measurements with Verifire interferometer

Unlike the DynaFiz, the Verifire interferometer employs a well-known acquisition technique based on phase shifting interferometry (PSI) (see, for example, Refs. [19,20] and references therein). In PSI, multiple intensity fringe patterns are recorded by sequentially shifting the transmission reference in well-defined steps by means of a piezo-actuator. The recorded fringe patterns are used to evaluate the OUT height at each pixel.

For PSI measurements, tilting the OUT leads to an increase of the number of fringes, the spatial resolution (number of pixels per fringe) of each fringe, corresponding to the change of the optical path in the test wavefront by $2\pi$, effectively decreases. The degradation of the fringe resolution can, potentially, lead to an increase in the error of the test surface height evaluation from the series of the fringe patterns recorded in the interferometer PSI mode. This error contributes to the measured value of the surface roughness, and, therefore, to the measured PSD distributions.

At first glance, because the surface height value is estimated for each pixel, one can expect that at the uniformly tilted plane test surface, the tilt-related error of the height evaluation must be randomly distributed. Correspondingly, the PSD distribution measured with the tilted test surface will have a constant level shift compared with the untilted surface PSD.

However, as we know (see, for example, Refs. [3-7]), the test surface tilt is associated with increased retrace error, when the test wavefront is effectively shifted laterally with respect to the reference wavefront, leading to distortion in the interference fringe pattern. Correspondingly, the mutual shift of the reference and the test wavefronts with respect to the detector pixel grid can lead to additional error of the height evaluation for each pixel. This height evaluation error may depend on lateral position and spatial frequency. With the increased density of the fringe patterns due to the test surface tilt, the lateral wavefront shift can also significantly affect the random error in the height evaluation.

Moreover, a strong astigmatism in the retrace error pattern, discussed in Ref. [6], which was simulated by a small decenter misalignment of one of the lens elements of the transmission reference optics, can lead to an effective astigmatism in the tilt-related PSD distortion measurements.

Below, we present preliminary results of an experimental test of the tilt-related PSD distortion mechanism hypothesized here. These efforts can be considered as the first, but important, step in developing a data acquisition and data processing methodology for precision stitching Fizeau interferometry with aspherical x-ray optics while mitigating the ITF distortions we have observed.

### 2.3 PSD Measurements of with Verifire interferometer with sample at different vertical tilts

Figure 3 shows the PSD in the X and Y directions of a 25-μm HR BPRA at different horizontal tilts measured with the Verifire interferometer and evaluated with Zygo Mx software (compare with Ref. [6]). As already pointed out in Sec. 2.1, the tilt dependence of the PSD (and, therefore, that of the ITF) obtained with the Verifire interferometer (Fig. 3) is significantly different compared to that of the DynaFiz interferometer. Thus, with tilting the sample in both the positive and the negative X directions, the 1D PSDX and PSDY increase; the increase is monotonic with the magnitude of the tilt; and there are no bumps that characterize the measurements with the DynaFiz.

The dependence of the PSD distortion on the value of the HR BPRA sample tilt in the horizontal direction is depicted in Fig. 4, where the PSD distortions are calculated by subtracting the baseline PSD [Fig. 3(c)] from the PSD distributions measured with the tilted HR BPRA sample [Fig. 3(a,b,d,e)].

The PSDX and PSDY distortions caused by tilting the HR BPRA sample in the horizontal direction (Fig. 4) are in qualitative agreement with the tilt-related PSD distortion mechanism suggested in Sec. 2.2 associated with an increase in the random and systematic errors of height evaluation in the PSI mode of a Fizeau interferometer. Indeed, as expected, distortion of the PSD in the direction of the tilt [Fig. 4(a)] has a close-to-random character for the middle-to-high spatial frequency range, and its magnitude is significantly larger than that of the PSDY distortion [Fig. 4(b)]. The observed spatial frequency dependence of the PSD distortion and its strong asymmetry between PSDX and PSDY can be attributed to retrace error with a strong astigmatism of the error pattern (see Sec. 2.2).

However, the results presented in Fig. 4 raise some additional questions. Mainly, there is an unexpected, many orders of magnitude, difference between the PSDX and PSDY distortions at low spatial frequencies, where the distortion in the direction of the tilt is much smaller than in the direction orthogonal to the tilt. A possible explanation could be a small deviation of the tilt rotation axis from the perfect vertical (Y) direction. In this case, the dense pattern of the vertical oriented interference fringes is slightly misaligned with respect to the vertical axis, leading to a lower frequency error of the PSDY evaluation.

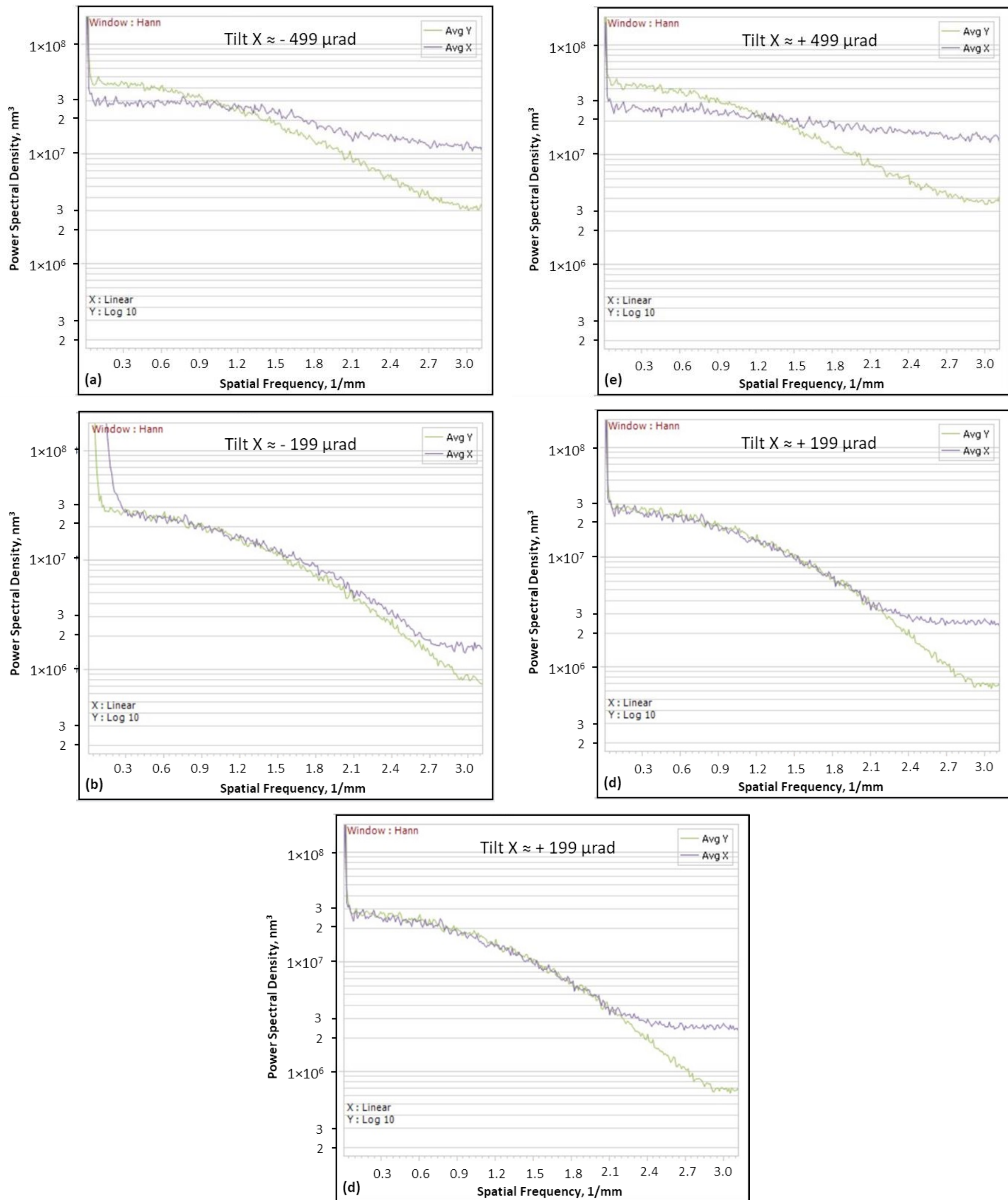


Figure 3. Verifire measurements (using 6th order detrending) of the PSD in the X (violet lines) and Y (green lines) directions measured with the 25-µm HR BPRA test sample at different horizontal tilts of (a) -499 µrad, (b) -199 µrad, (c) -2.8 µrad (baseline), (d) +199 µrad, and (e) +499 µrad.

Note that in the case of the measurements depicted here, the effective surface tilt magnitude in the vertical direction was less than 1-2 µrad. The low spatial frequency surface slope variation that, for the sample in use, is on the level of a few microradians can also contribute to the low-spatial-frequency distortion of the PSD.

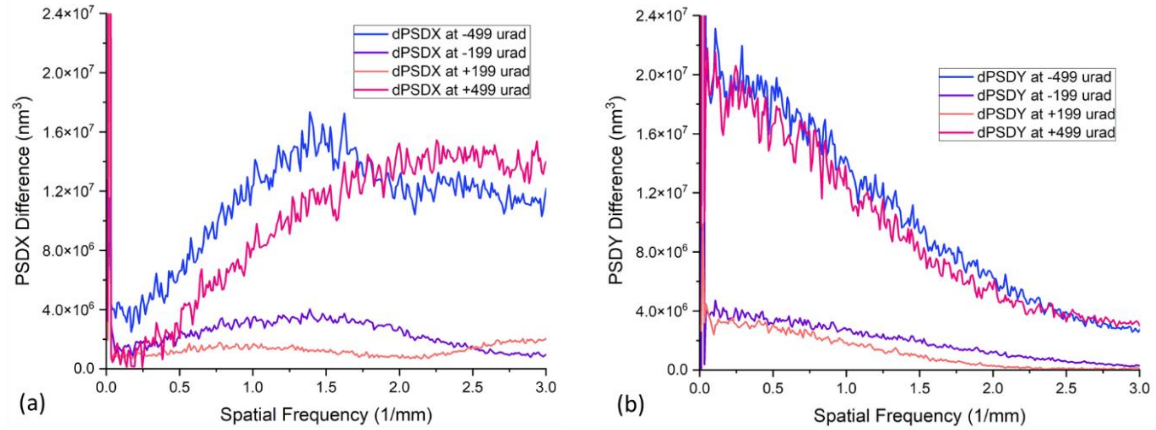


Figure 4. Changes in (a) PSDX and (b) PSDY seen in Verifire measurements with horizontal tilt, found by subtracting the baseline PSD [Fig. 3(c)] from the PSD with tilt [Fig. 3(a,b,d,e)].

If this explanation above is correct, the tilt dependence of the PSD measured with a HR BPRA sample could be a powerful method for high accuracy alignment of the tilting and translation stages used in the stitching interferometry setups. We plan additional dedicated experiments to check this hypothesis.

### 2.4 PSD measurements of 120-m ROC cylindrical Si substrate

Here, we discuss preliminary results concerning tilt-related distortion of PSD measurements obtained with a cylindrical super-polished Si substrate available at the ALS XROL. The sample substrate of 150 mm length [Fig. 5(a)] with tangential radius of curvature of 120 m was used to measure the retrace error. Data presented here was taken with the Verifire interferometer configured with a 34 mm optical cavity [Fig. 5(b)].

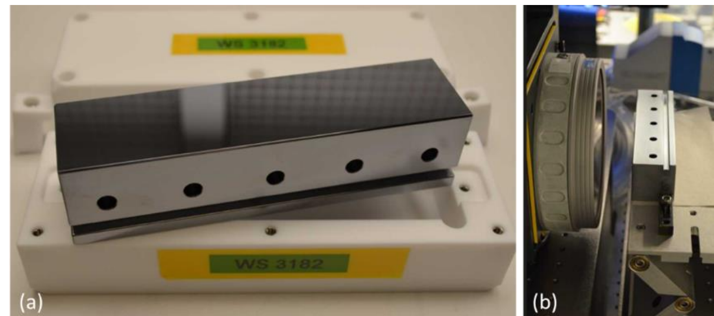


Figure 5. (a) 120-m ROC Cylindrical Substrate and (b) the experimental arrangement with a 34 mm optical cavity.

Figure 6 shows the plane-detrended Verifire measurement of the 120-m cylindrical substrate, while Fig. 7 shows the residual height profiles of the substrate in the direct and flipped orientations after the best-fit cylindrical surface has been subtracted. If the observed residual profile, with peak-to-valley (PV) variation of about 120 nm, were due to the substrate, it would flip upon flipping the substrate. Because it is the same for both measurements, it must be due to retrace error.

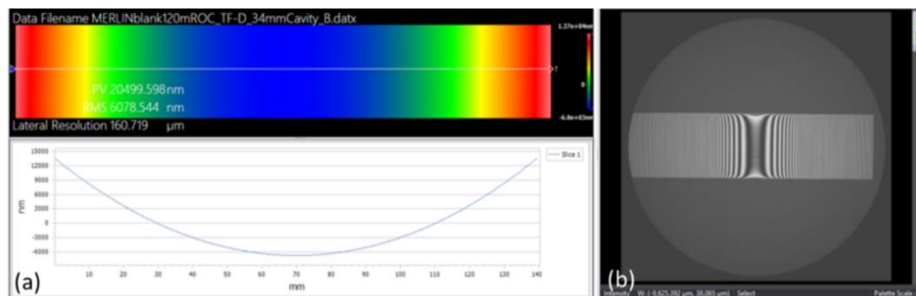


Figure 6. (a) The plane-detrended surface height profile of the cylindrical substrate and its tangential cross-section (lower plot) as measured with the Verifire. (b) The corresponding intensity fringe pattern.

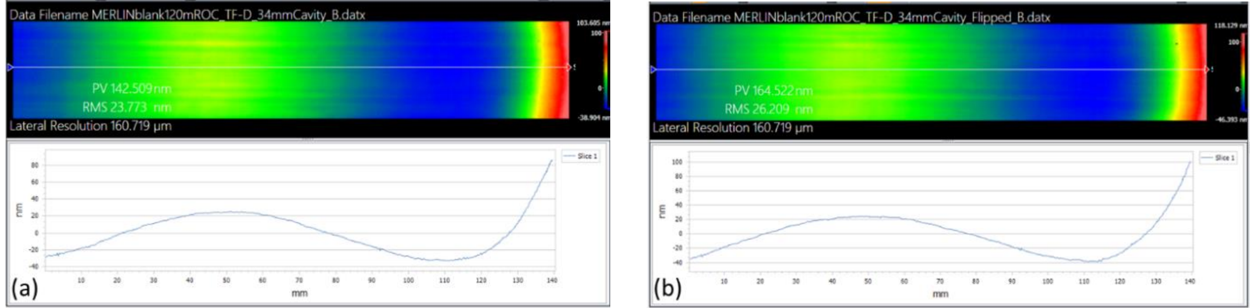


Figure 7. Surface height profile after cylindrical detrending with the substrate in the (a) direct and (b) flipped orientations.

The contribution to the measured profile that is due to the actual surface shape can be identified from the difference of the height profiles recorded with the substrate in the direct and flipped configurations (Fig. 8). The PV variation of the difference cross-section trace is only about 10 nm, an order of magnitude smaller than the retrace error. Note that half of the PV variation of the difference is an estimate of the PV variation of the substrate profile.

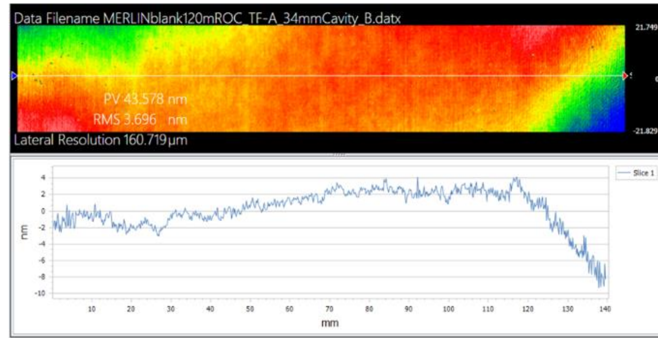


Figure 8. Difference between the plane-detrended surface height profiles of the cylindrical substrate measured in the direct and flipped orientations.

For comparison, Fig. 9 presents the results of high-accuracy surface slope measurement with the same 120-m cylindrical substrate performed with the XROL Optical Surface Slope System (OSMS) [21,22]. The residual (cylindrically detrended) height profile obtained via integration of the slope profile in Fig. 9(a) is shown in Fig. 9(b). The PV variation of the height profile is about 3.6 nm, in good agreement with half of the PV value of the difference cross-section trace in Fig. 8.

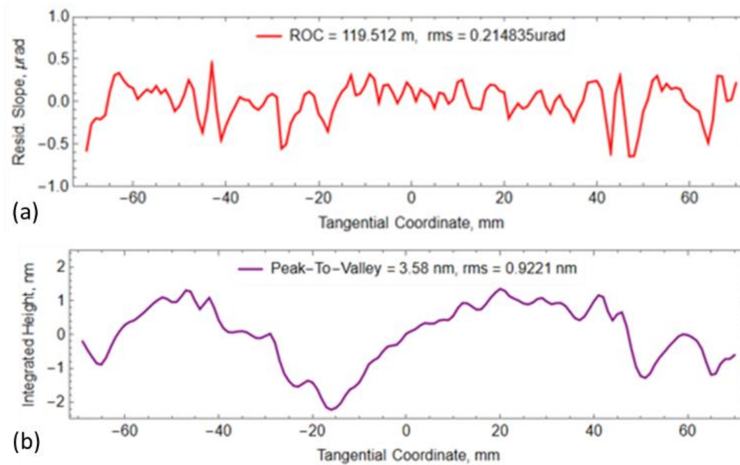


Figure 9. (a) The residual (cylindrically detrended) surface slope trace along the tangential direction of the cylindrical substrate measured with the OSMS; and (b) the residual height variation obtained by numerical integration of the slope trace data.

The total surface slope variation of the cylindrical substrate, shown in Fig. 9(a), is about ± 0.6 mrad. Therefore, in analogy with the result of the PSD measurements with the tilted HR BPRA test sample in Sec. 2.3, one can expect that the PSD measured over differently tilted areas of the substrate will depend significantly on the effective tilt. In order to test this assumption, we selected 5 different areas with masks (Fig. 10) and evaluated PSDs for each area - Figs. 11 and 12.

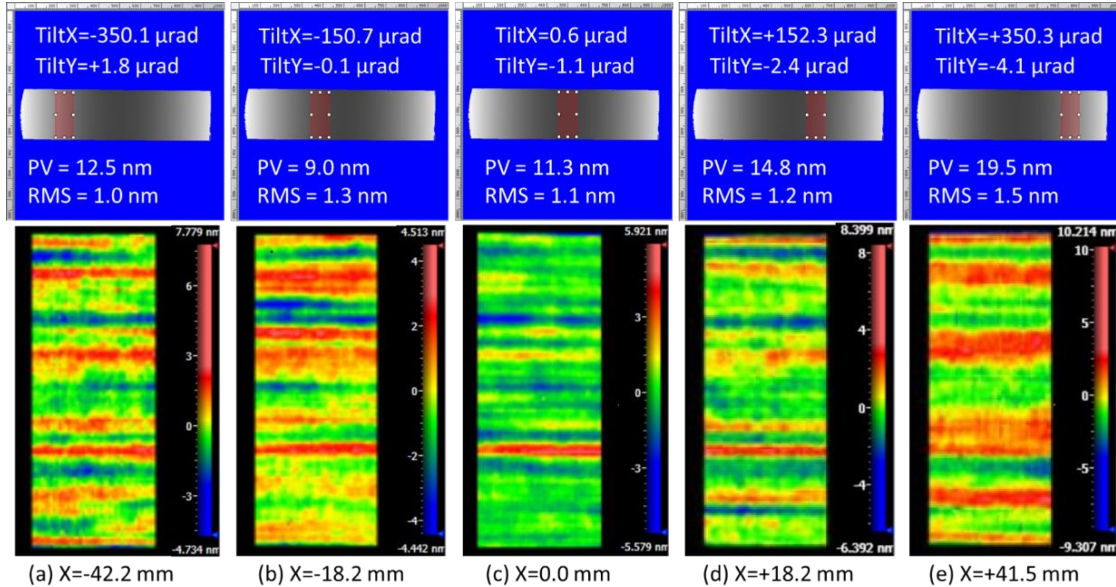


Figure 10. (Top row) masks and (bottom row) height profiles of the masked areas of the Verifire measurement depicted in Figure 10(a). The effective tilts of the masked areas of the cylindrical substrate, and the PV and RMS variations, were obtained using piston and -order detrending, respectively. The center X position of each area is given with respect to the central area.

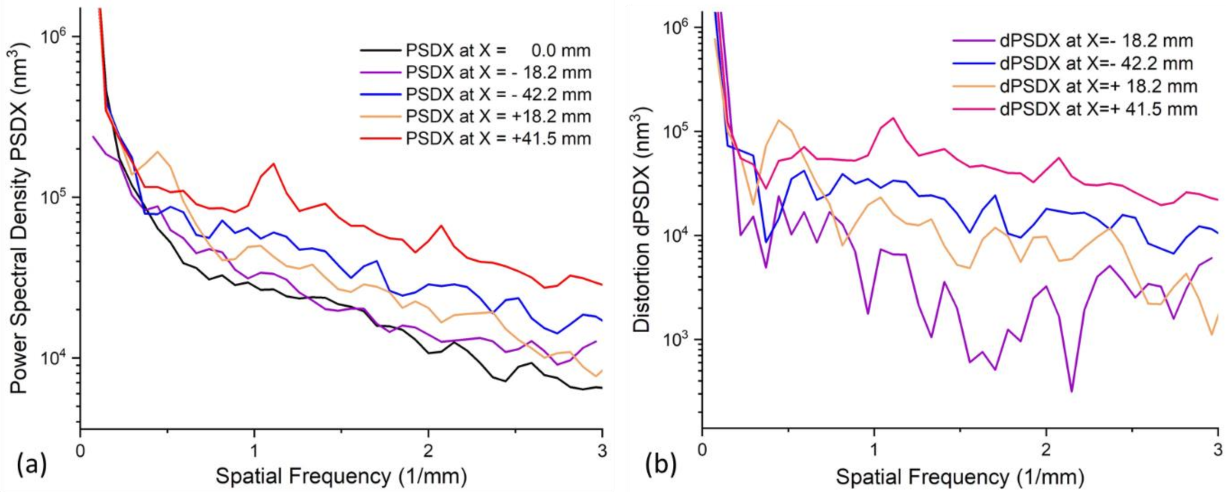


Figure 11. (a) PSDX evaluated in Mx for the different masked areas of the cylindrical substrate as in Figure 13; (b) PSDX distortions dPSDX calculated by subtraction of the PSDX of the substrate central area from the PSDX corresponding to the tilted subareas of the 120-m cylindrical substrate.

As with the PSD measurements of the tilted 25-µm HR BPRA test sample, we have the important result that there is a strong dependence of the measured PSD on the tilt of the OUT. Similar to the result in Fig. 4(a), the PSDX distortions in Fig. 11(b) have a close to random character over the middle-to-high spatial frequency range that is also in qualitative agreement with the tilt-related PSD distortion mechanism suggested in Sec. 2.2.

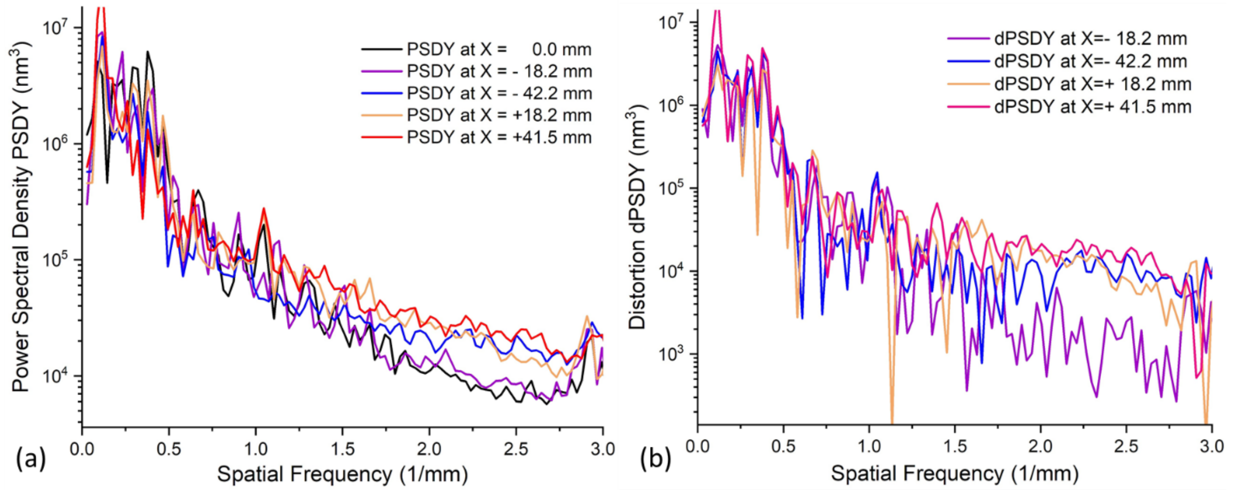


Figure 12. PSDY and dPSDY as for Figure 11.

In the PSD measurements with the cylindrical substrate, we see a strong difference of the PSDX and PSDY distortions [compare Fig. 11(b) and Fig. 12(b)] that is also in a qualitative agreement with the PSD distortion observed with the HR BPRA sample. But in this case, the strong asymmetry of the substrate topography in the X and Y direction (refer to the height distribution images of the selected subareas in Fig. 10, the bottom row) also contributes to the difference and subarea-to-subarea variation of the PSDX and PSDY.

However, the more detailed comparison reveals some significant differences that we cannot reliably attribute to some particular distortion mechanism. This may relate to the cylindrical shape of the substrate. When comparing the tilt-related distortion of the PSDs measured with the HR BPRA sample and observed with the cylindrical substrate, we should consider the monotonic variation of the tilt angle across the particular area of the substrate. For the selected masks, the variation is about ±50 µrad.

As with the other observations of the dependence of PSD on sample tilt discussed above, further investigation is required to conclusively establish the true source of the distortion.

## 3. PSDS IN ZYGO MX SOFTWARE USING ANNULAR MASKS

In Sec. 2, we discussed possible sources of distortion of the PSD measurement related to the instrument, the experimental setup, and the OUT itself. It is also important to be aware of details of the algorithm for calculating the PSD (e.g., normalization conventions) that can potentially produce misleading results.

Most users of Zygo metrology tools use the Zygo Mx software for data analysis as well as data acquisition. However, as we show in this section, the conventions used in Mx for evaluation of the PSD may not be appropriate for all tasks related to ITF calibration using measurements of BPRA targets.

For the tests discussed below, we use measurements of the 25-µm HR BPRA test sample recorded with the Verifire Fizeau interferometer. We do not present here the similar tests performed with the data obtained with the DynaFiz interferometer because the results of those tests are equivalent to the ones presented here.

Analysis of Verifire measurements of the 25-µm HR BPRA sample are shown in Fig. 13 using piston detrending and in Fig. 14 using (a) plane and (b) 6th-order polynomial detrending. The higher order detrending decreases the magnitude of the PSD at low spatial frequencies, and does not noticeably affect the PSD at the middle and high spatial frequencies. The roll-off in the higher spatial frequencies that is an indication of the limited spatial resolution of the interferometer is also not changed by detrending. Similar comparison tests were performed to ensure that other data-processing options in Mx, such as filling of missing data points, do not affect the PSD at the middle and high spatial frequencies especially important for the ITF calibration.

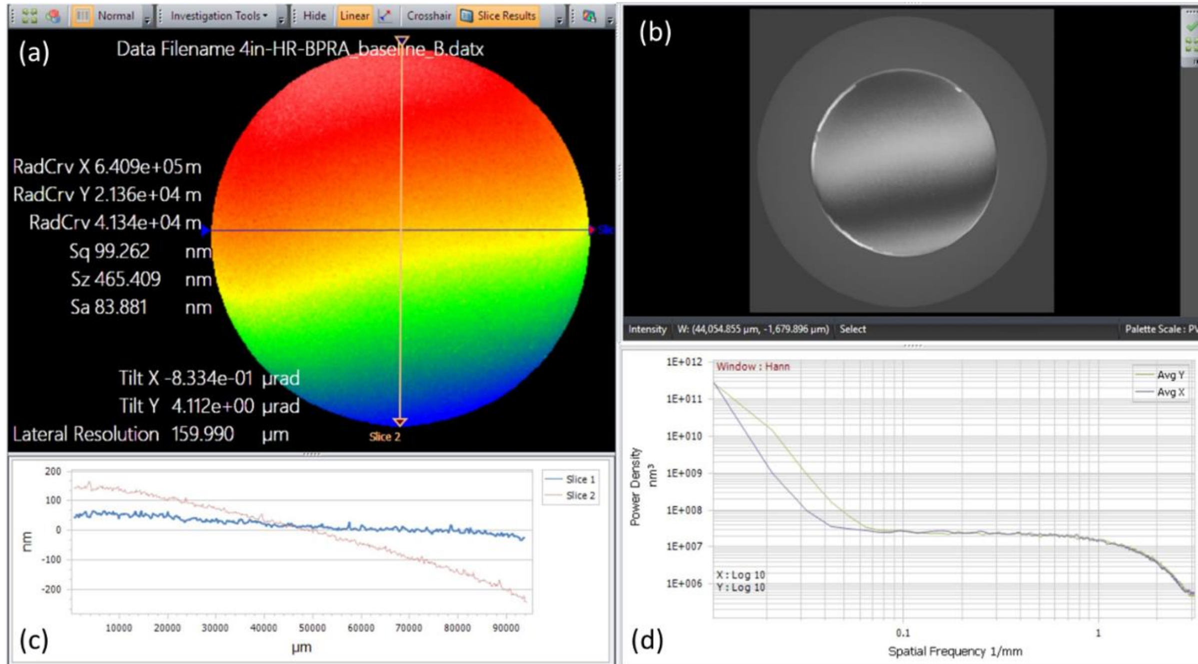


Figure 13. Screenshots of Mx software depicting (a) the Verifire surface-height measurement of the 25-µm HR BPRA sample (piston detrended), (b) the intensity fringe pattern, (c) horizontal and vertical cross-sections of the height profile, and (d) the averaged PSD in the horizontal and vertical directions.

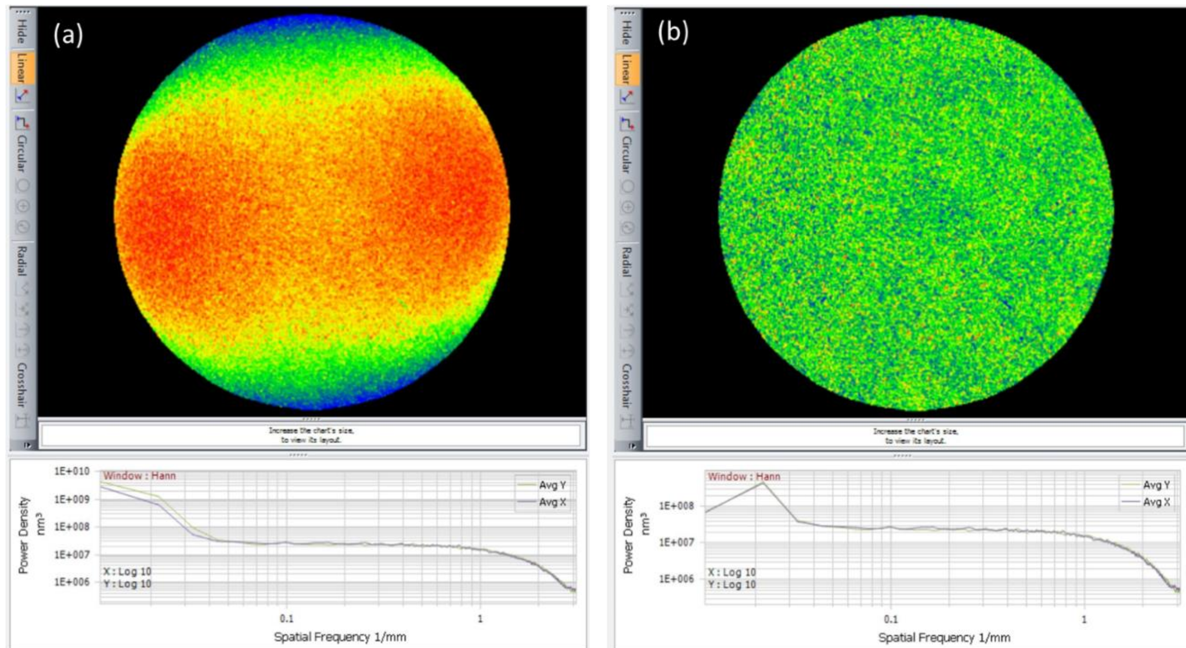


Figure 14. Mx screenshots of the same data as in Fig. 13, but with (a) plane and (b) 6th-order polynomial detrending.

To analyze possible position dependence of the ITF, in particular, a possible dependence on the distance from the center of the measurement, we used the Mx masking functionality to analyze the same data (with 6$^{th}$-order polynomial detrending) cropped with the annular masks depicted in Fig. 15.

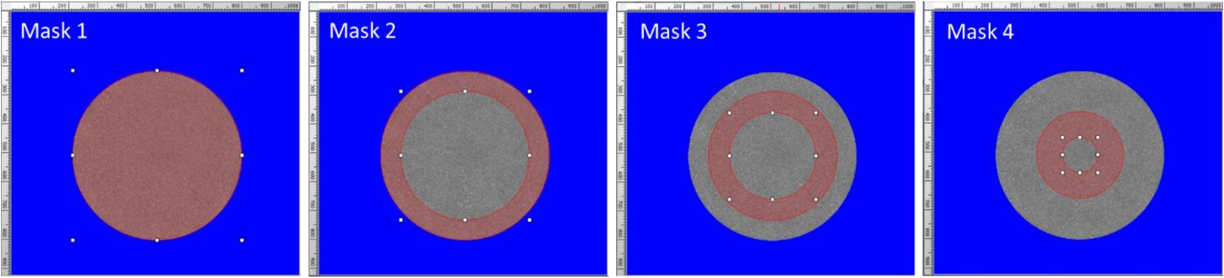


Figure 15. The circular (Mask 1) and annular masks used for reprocessing the data shown in Fig. 14(b). The circular mask was also used in processing the data shown in Fig. 13 and Fig. 14.

Figure 16 shows the masked height profiles and corresponding 1D PSDs in the horizontal and vertical directions.

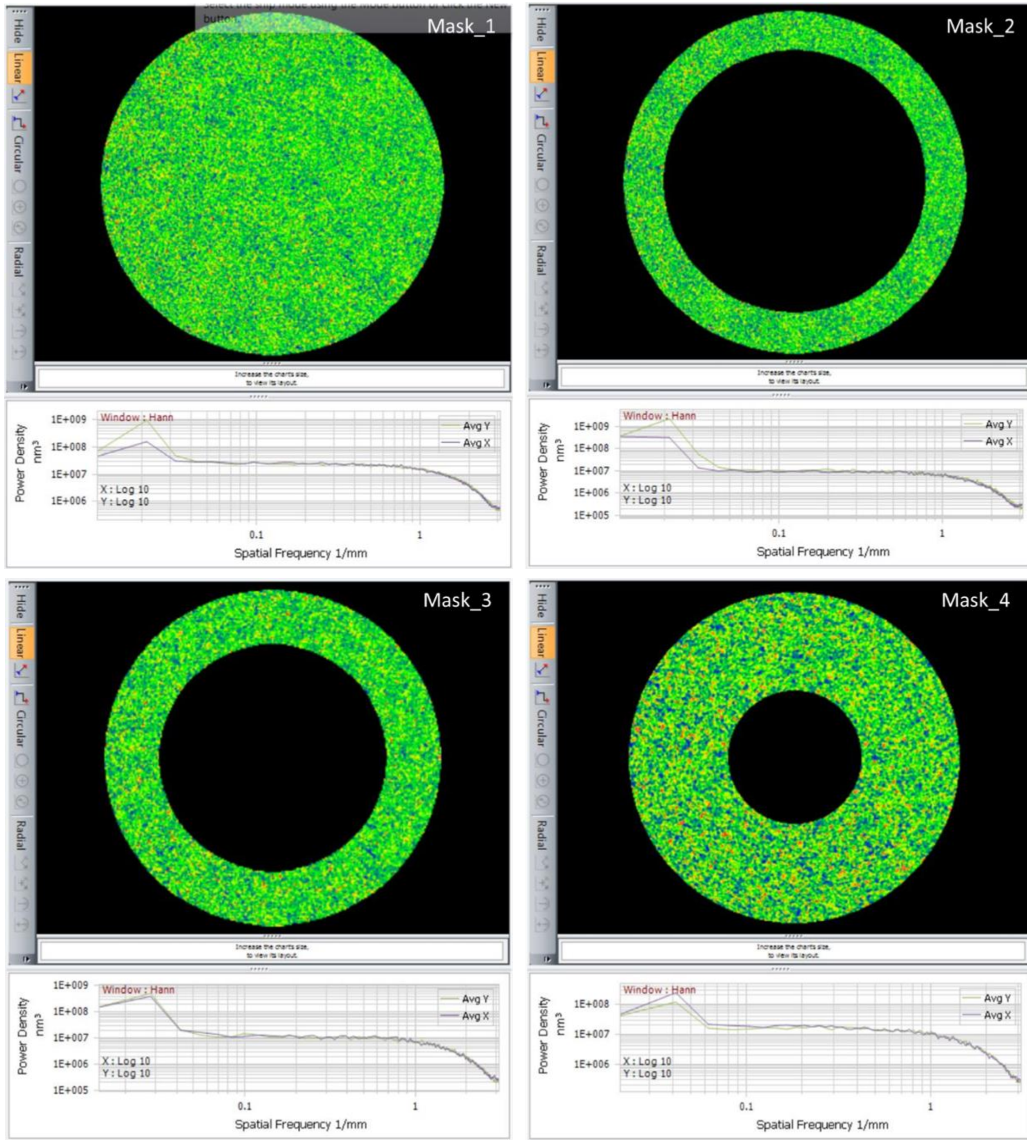


Figure 16. Surface height data with circular and annular masks depicted in Fig. 15 and corresponding horizontal and vertical 1D PSDs.

The qualitative shape of each PSD in Fig. 16 is the same, independent of the mask used. However, the PSD magnitude does depend on the mask – comparing the PSDs at middle and high frequencies shows that, compared to the circular mask 1, the annular masks 2, 3, and 4 have PSDs scaled down by factors of approximately 2.5, 2.1, and 1.45, respectively. On the other hand, PSDs obtained with different-sized circular and rectangular masks have approximately the same magnitude, independent of the mask size. Thus, we surmise that, to find the PSD of a masked image, Mx takes the PSD over the rectangular bounding box of the mask, setting points outside the mask (but inside the bounding box) to zero. Crucially, it appears that no normalizing factor is included for non-rectangular masks to correct the PSD magnitude according to the fraction of the bounding box that is masked.

Annular masking of data recorded by Fizeau interferometers with axial symmetry is important to analyze possible radial dependences in the results. Because no correction factor for annular masks is included in Mx, PSDs calculated using such masks in Mx will obscure the true radial dependence unless corrections are made by hand. For example, in the case considered here, there is no significant radial dependence of the ITF, even though a naive reading of the PSD results would indicate a strong dependence.

As a confirmation of our conclusion that the Mx software limitation relates to the PSD evaluation over annular areas, we present also the results of the Mx software application to the PSD measurements over different square areas cropped from the same measurement after 6th-order polynomial detrending as depicted in Fig. 14(b), above.

Figure 17 presents the surface height data with two square masks and corresponding horizontal and vertical 1D PSDs.

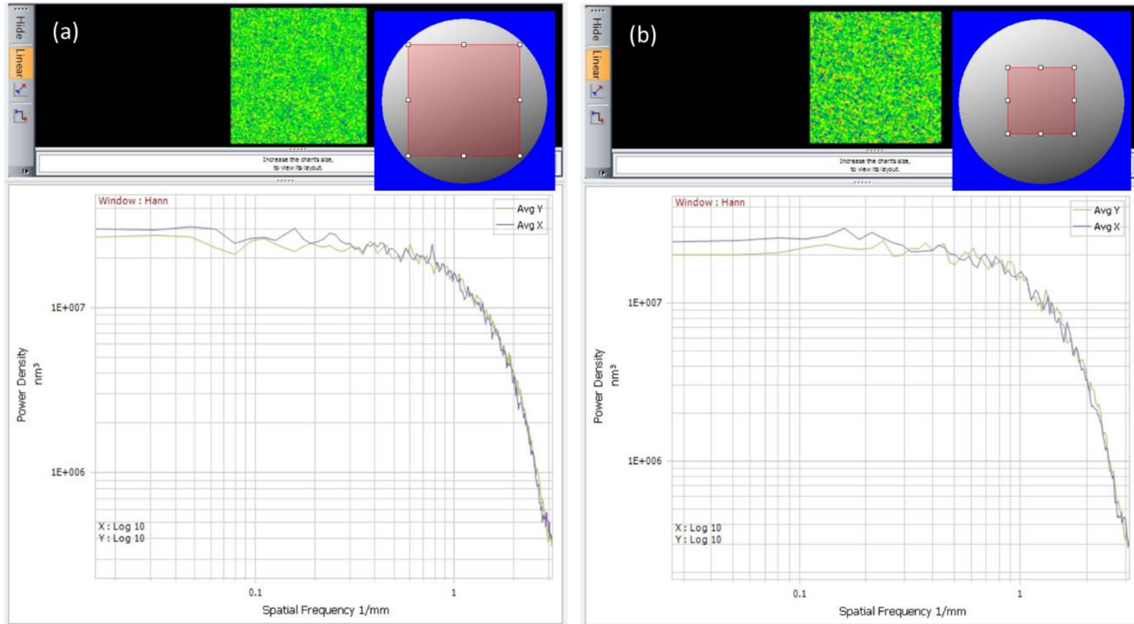


Figure 17. Mx screenshots of the surface height data in Fig. 14(b), cropped with two square masks, depicted in the insets, and corresponding horizontal and vertical 1D PSDs.

For the both square masks, the magnitude of the PSD at the middle and high spatial frequencies, as well as the high frequency roll-off do not noticeably differ from that of the circular area PSD in Fig. 14(b). Note that the ratios of the entire circular area to the masked ones in Fig. 17 are (a) 1.72 and (b) 4.86. The same result was obtained with smaller circular mask similarly scaled compared to the whole circular area.

## 4. SOFTWARE DEVELOPMENT

### 4.1 PSD evaluation

For this project we are developing our own ITF calibration software for analysis of the BPRA measurement. It can find the 2D, average 1D, and azimuthally averaged PSD using either smooth or boxcar rectangular, circular, or annular

windows. Normalization by the sum over the square of the window function is used, which means that the PSD of a uniform image will have the same magnitude for any window size or shape, including for annular windows.

Figure 18 shows screenshots of our software applied to the same data considered above with windows corresponding to masks 1 and 2 depicted in Fig. 15. Our software finds PSDs of the same magnitude for both the circular and annular windows (see also Fig. 20), as compared to a factor of ~2.5 difference using corresponding masks in Mx (Sec. 3).

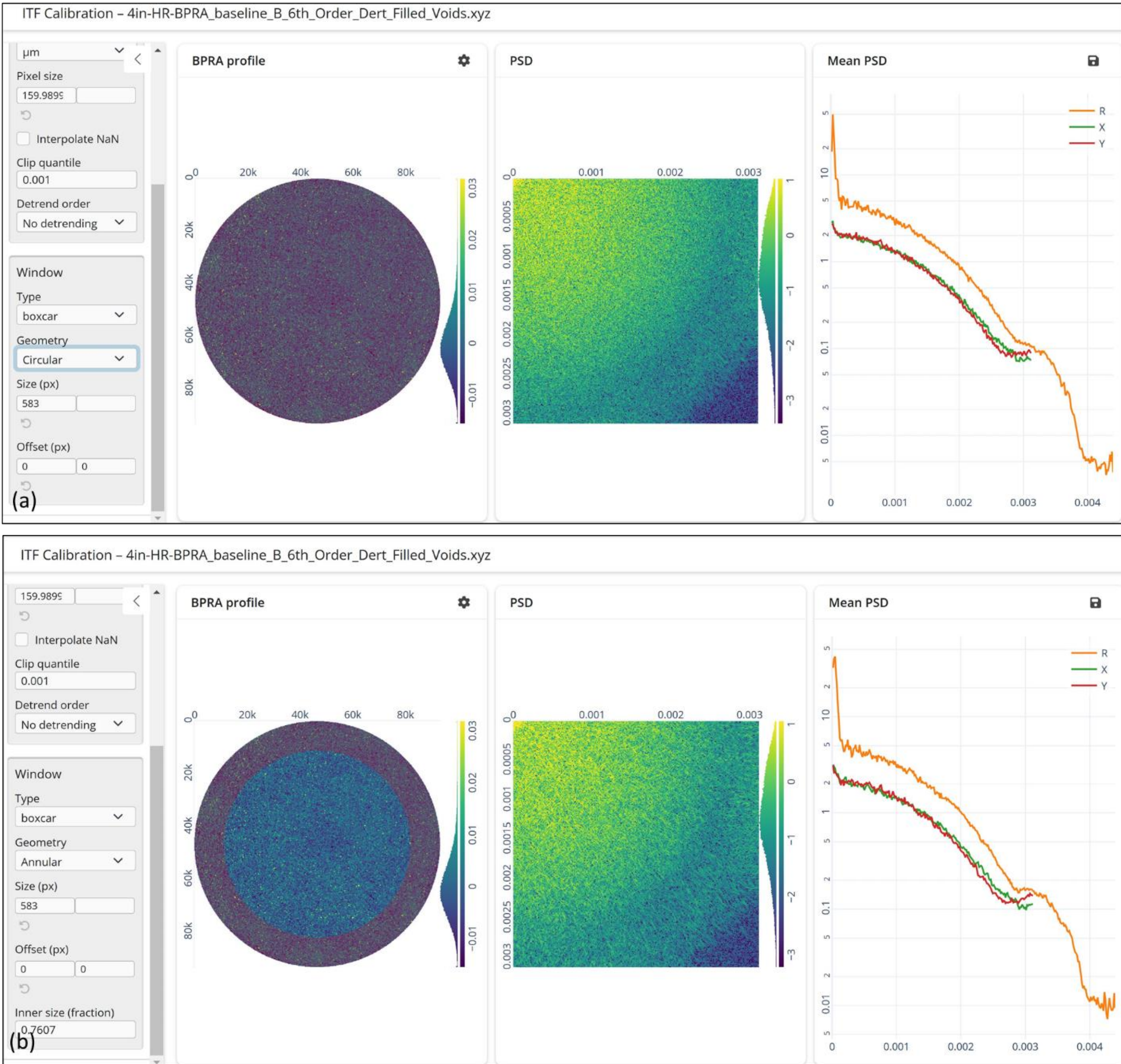


Figure 18. Screenshot of our software using windows matching (a) the circular mask 1 and (b) the annular mask 2 depicted in Fig. 15.

Figure 19 compares the PSDs obtained using the circular and annular windows. The differences in Fig. 19 (a-c) are primarily due to the annular mask used to crop the circular area data. Because the annular mask has a longer total border length than the circular window, the step-function-like height variation at the border of the window has a relatively larger impact on the resultant PSD for the annular window compared to the circular. This results in a difference between the circular and annular window 1D PSDs with approximately *1/f* character (similar to that of the step function), where *f* is the spatial frequency, as seen in Fig. 19 (d).

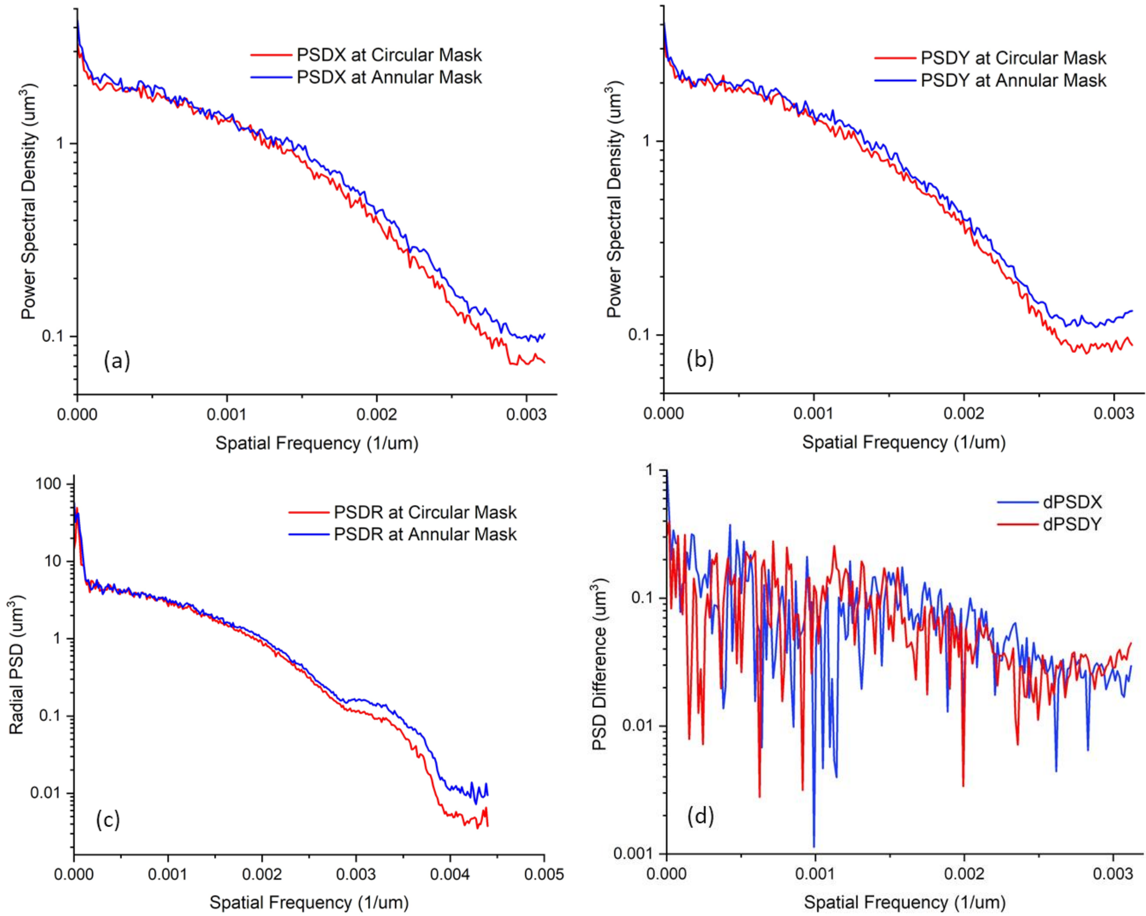


Figure 19. (a) PSDX, (b) PSDY, (c) PSDR and (d) the difference between PSDX and the difference between PSDY evaluated with circular and annular windows.

For the PSD data processing in Fig. 19, the boxcar window was chosen to most closely match the Mx masks. We have checked that indeed, there is a noticeable difference at high spatial frequencies between the 1D PSD distributions evaluated with our software with the boxcar-like window and a smooth window type, such as the Hann window – Fig. 20.

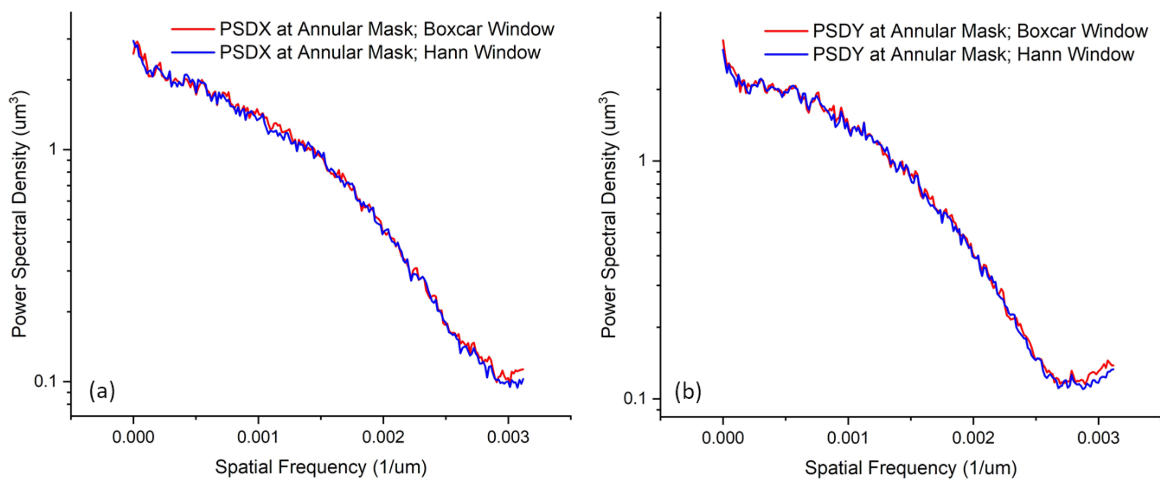


Figure 20. (a) PSDX and (b) PSDY evaluated with annular windows using the boxcar-like (the red lines) and the Hann window (the blue lines). There is a noticeable difference at high spatial frequencies between the 1D PSD distributions evaluated with the boxcar-like and the Hann windows.

The above shows that, for this application, our software is a more appropriate PSD evaluation tool than Mx. We will continue to extend our software with algorithms specifically tailored to the tasks involved in ITF calibration and the other surface reconstruction techniques under development in this project.

## 5. DISCUSSION AND CONCLUSIONS

Working on project in progress to develop precision stitching Fizeau interferometry metrology with long tangentially curved x-ray mirrors (see also Refs. [5,6]), we pinpointed critical issues with current SPWFI techniques, including retrace error, geometrical distortion, and limited spatial resolution. Additionally, we created a suite of original test artifacts, including the highly HR and URA binary-pseudo BPRA standards. These standards are optimized for comprehensive and precise calibration of Fizeau interferometers.

Using our calibration standards and techniques, we tested the performance of the ALS XROL Fizeau interferometers. Our experimental data, analyzed with custom data processing and simulation software, revealed a complex interplay of spurious effects, including retrace error, geometrical distortion, and apparent dependence of the PSD of the OUT on the alignment and shape of the OUT discussed in the present report. Comparing our custom software for evaluating PSDs to the commercial equivalent, we found that the commercial software can produce misleading results for certain applications.

Reliable and accurate SPWFI will require calibration of the interferometer in the specific experimental arrangement used for SPWFI measurements and data reconstruction to address the sources of error discussed in this paper. Our adaptive, OUT specific, calibration technique involves variable-shape calibration artifacts, such as a bendable test artifact system. Our next steps are the integration of the bendable test system with the ALS XROL Verifire™ Fizeau interferometer and experimental investigations of the OUT curvature dependence of the retrace error, geometrical distortion, and PSD distortion.

## ACKNOWLEDGEMENTS

The authors are grateful to Ulf Griesmann for fruitful discussions. This work was partially supported by the U.S. Department of Energy Office of Science, Office of Basic Energy Sciences, and Small Business Technology Transfer (STTR) programs under Award Numbers DE-SC0011352, DE-SC0022373, and DE-SC0022412 to HighRI Optics, Inc. and Rochester Scientific, LLC. Research at the Advanced Light Source and the Molecular Foundry at Lawrence Berkeley National Laboratory are supported by the Office of Science, Office of Basic Energy Sciences, and Material Science Division of the U.S. Department of Energy under Contract No. DE-AC02-05CH11231.

## DISCLAIMER

This document was prepared as an account of work sponsored by the United States Government. While this document is believed to contain correct information, neither the United States Government nor any agency thereof, nor The Regents of the University of California, nor any of their employees, makes any warranty, express or implied, or assumes any legal responsibility for the accuracy, completeness, or usefulness of any information, apparatus, product, or process disclosed, or represents that its use would not infringe privately owned rights. Reference herein to any specific commercial product, process, or service by its trade name, trademark, manufacturer, or otherwise, does not necessarily constitute or imply its endorsement, recommendation, or favor by the United States Government or any agency thereof, or The Regents of the University of California. The views and opinions of authors expressed herein do not necessarily state or reflect those of the United States Government or any agency thereof or The Regents of the University of California.

## REFERENCES

[1] H. Mimura, H. Yumoto, S. Matsuyama, K. Yamamura, Y. Sano, K. Ueno, K. Endo, Y. Mori, M. Yabashi, K. Tamasaku, Y. Nishino, T. Ishikawa, K, Yamauchi, "Relative angle determinable stitching interferometry for hard x-ray reflective optics," Rev. Sci. Instrum. 76, 045102 (2005); https://doi.org/10.1063/1.1868472.

[2] P. de Groot, J. Kramer, T. Sutherland, "Modeling the topographic lateral resolution of interferometers," Proc. of SPIE Vol. 12619, 126190N (2023); doi: 10.1117/12.2670939.

[3] C. Hu, L. Chen, D. Zheng, Y.Wang, Z. Ma, and Z. Zhang, "Iterative correction method of a retrace error in interferometry," Optics Express 30, 37619-37636 (2022); https://doi.org/10.1364/OE.469341.
[4] C. Kreischer, "Retrace error: interferometry's dark little secret," Proc. of SPIE 8884, 88840X (2013); doi: 10.1117/12.2029324.
[5] Morrow, K., da Siva, M. B., Alcock, S., "Correcting retrace and system imaging errors to achieve nanometer accuracy in full aperture, single-shot Fizeau interferometry," Opt. Express 31(17), 27654 (2023); https://doi.org/10.1364/OE.498043.
[6] K. Munechika, K. Yamada, S. Rochester, H. Barnard, W. Chao, I. Lacey, C. Pina-Hernandez, P. Z. Takacs, and V. V. Yashchuk, "Binary pseudo-random array standards for calibration of 3D optical surface profilers used for metrology with significantly curved x-ray optics," the SPIE Optics and Photonics 2024, Conference OP500: Advances in X-Ray/EUV Optics and Components XIX, Symposium: OP24O SPIE Optical Engineering + Applications, Paper 13150-14, (18 - 22 August 2024, San Diego, California, United States); this conference.
[7] K. Munechika, S. Rochester, W. Chao, I. Lacey, C. Pina-Hernandez, D. Padmore, K. Yamada, V. V. Yashchuk, P. Z. Takacs, M. P. Biskach, A. Numata, "Binary Pseudo-random Array (BPRA) for Inspection and Calibration for Cylindrical Wavefront Interferometry," the SPIE Optics and Photonics 2024, Conference OP323: Interferometry and Structured Light 2024, Symposium: OP24O SPIE Optical Engineering + Applications, Paper 13135-4, (18 - 22 August 2024, San Diego, California, United States); this conference.
[8] Boreman, G. D., [Modulation Transfer Function in Optical and Electro-optical Systems], SPIE Press, Bellingham, Washington (2001).
[9] Foreman, M. R., Giusca, C. L., Coupland, J. M., Torok, P., Leach, R. K., "Determination of the transfer function for optical surface topography measuring instruments - a review," Meas. Sci. Technol. 24, 052001/1-18 (2013); doi:10.1088/0957-0233/24/5/052001.
[10] de Groot, P. J., "The instrument transfer function for optical measurements of surface topography," J. Phys. Photonics 3, 024004/1-16 (2021); doi: https://doi.org/10.1088/2515-7647/abe3da.
[11] Yashchuk, V. V., McKinney, W. R., and Takacs, P. Z., "Test surfaces useful for calibration of surface profilometers," United States Patent No.: 8,616,044.
[12] Yashchuk, V. V., Anderson, E. H., Barber, S. K., Bouet, N., Cambie, R., Conley, R., McKinney, W. R., Takacs, P. Z., Voronov, D. L., "Calibration of the modulation transfer function of surface profilometers with binary pseudo-random test standards: expanding the application range to Fizeau interferometers and electron microscopes," Opt. Eng. 50(9), 093604 (2011); doi: 10.1117/1.3622485.
[13] V. V. Yashchuk, S. Babin, S. Cabrini, W. Chao, U. Griesmann, I. Lacey, S. Marchesini, K. Munechika, C. Pina-Hernandez, and A. Roginsky, "Binary pseudorandom array test standard optimized for characterization of large field-of-view optical interferometers," Proc. SPIE 11490, 114900W/1-8 (2020); doi: 10.1117/12.2568309.
[14] Yashchuk, V. V., Artemiev, N. A., Lacey, I., McKinney, W. R., and Padmore, H. A., "Advanced environmental control as a key component in the development of ultra-high accuracy ex situ metrology for x-ray optics," Opt. Eng. 54(10), 104104 (2015); doi: 10.1117/1.OE.54.10.104104
[15] Yashchuk, V. V., Babin, S., Cabrini, S., Griesmann, U., Lacey, I., Munechika, K., Pina-Hernandez, C., and Wang, Q., "Characterization and operation optimization of large field-of-view optical interferometers using binary pseudorandom array test standard," Proc. SPIE 10749, 107490R/1-13 (2018); doi: 10.1117/12.2322011.
[16] AMETEK/Zygo Corporation, "DynaFiz® Confident Metrology for a Dynamic World;" https://www.Zygo.com/products/metrology-systems/laser-interferometers/dynafiz.
[17] Takacs, P. Z., Li, M. X., Furenlid, K., and Church, E. L., "Step-height standard for surface-profiler calibration," Proc. SPIE 1995, 235–244. (1993); https://doi.org/10.1117/12.162661
[18] P. J. de Groot, Z. Daouda, L. L. Deck, and X. Colonna de Lega, "Linear systems characterization of the topographical spatial resolution of optical instruments," Appl. Opt. 63(15), 4201-4210 (2024); https://doi.org/10.1364/AO.521868.
[19] D. Malacara, M. Servín, and Z. Malacara, "Phase-detection algorithms," in Interferogram Analysis for Optical Testing, 2nd ed. (CRC Press, Taylor & Francis Group, 2005), Chap. 6
[20] P. J. de Groot, "A review of selected topics in interferometric optical metrology," Rep. Prog. Phys. 82, 056101/1-32 (2019); doi: 10.1088/1361-6633/ab092d.
[21] I. Lacey, K. Anderson, G. P. Centers, R. D. Geckeler G. S. Gevorkyan, A. Just, T. Nicolot, B. V. Smith, and V. V. Yashchuk, "The ALS OSMS – Optical Surface Measuring System for high accuracy two-dimensional slope metrology with state-of-the-art x-ray mirrors," Proc. SPIE 10760, 1076002/1-20 (2018); doi: 10.1117/12.2321347.
[22] V. V. Yashchuk, S. Rochester, I. Lacey, and S. Babin, "Super-resolution surface slope metrology of x-ray mirrors," Rev. Sci. Instrum. 91, 075113/1-11 (2020); doi: 10.1063/5.0005556.